Available online at www.sciencedirect.com
ScienceDirect
Journal of Catalysis 250 (2007) 25–32
JOURNAL OF CATALYSIS
www.elsevier.com/locate/jcat

Ionic-liquid-like copolymer stabilized nanocatalysts in ionic liquids I. Platinum catalyzed selective hydrogenation of *o*-chloronitrobenzene

Chao-xian Xiao, Han-zhi Wang, Xin-dong Mu, Yuan Kou *

PKU Green Chemistry Center, Beijing National Laboratory for Molecular Sciences, College of Chemistry and Molecular Engineering, Peking University, Beijing 100871, China

Received 16 February 2007; revised 22 April 2007; accepted 6 May 2007

Available online 28 June 2007

Abstract

An ionic-liquid-like copolymer was used to stabilize the platinum nanoclusters in ionic liquids. Catalytic performance was tested by the selective hydrogenation of *o*-chloronitrobenzene. Platinum catalysts Pt-I (5.1 nm) and Pt-II (1.7 nm) both exhibited excellent activity and selectivity for the reaction and were recycled with the activity and selectivity preserved. An unprecedented total turnover number (>25,900) was obtained on the Pt-II catalyst. Infrared spectroscopy, transmission electron microscopy, X-ray diffraction characterizations, and density functional theory calculations were used to study the catalysts.

Keywords: Platinum nanoparticles; Nanocluster; Colloid; Quasi-homogeneous; Molten salts; Density functional theory calculations; Ostwald ripening; Recycle; Deactivate

1. Introduction

The hydrogenation of *o*-chloronitrobenzene (*o*-CNB) catalyzed by soluble platinum nanoparticles (or nanoclusters [1–16]) has been widely investigated over the last several decades [17–21]. *o*-Chloroaniline (*o*-CAN), an important intermediate in the chemistry of dyes, drugs, herbicides, and pesticides, is the desired product. Platinum nanoparticles have been found to be an effective catalyst, whereas a conventional polymer, poly(*N*-vinyl-2-pyrrolidone) (PVP), is usually used as the stabilizer to protect the particles. This PVP–Pt catalytic system has some serious drawbacks, however: (1) methanol usually used as the solvent for the reaction is toxic, volatile, and not green; (2) recycling of the expensive platinum catalyst is impossible due to the difficulty in the product separation; (3) the catalyst has very poor selectivity (∼46%), rising mainly from the undesirable dehalogenation and coupling reactions; and (4) a very low turnover frequency (TOF) is obtained. Consequently, development of a green, recyclable catalytic system with high selectivity and a large total turnover (TTO) number is of particular importance.

Ionic liquids (ILs), a class of molten salts with low melting points (<100 °C), should be an ideal choice for the improvement of the above-mentioned system. ILs have an extremely low vapor pressure, a wide liquid range, tunable polarity, and potentially easy recyclability [22–28]. ILs serve as green solvents for the replacement of methanol. Furthermore, because ILs comprise cations and anions, an additive electrostatic stabilization effect on the nanoparticles [13,29], together with an improved selectivity for the reaction [30], particularly to the hydrogenation of chloronitrobenzene [31], can be expected.

Direct transfer of PVP–Pt catalyst into ILs is difficult, however. The main problem is the poor solubility of the PVP polymer [15]. Therefore, designing an appropriate stabilizer that can act as well as that of PVP but can be readily dissolved in ILs is a key issue. We have recently reported that an IL-like copolymer (poly[(*N*-vinyl-2-pyrrolidone)–*co*–(1-butyl-3-vinylimidazolium chloride)], abbreviated as poly(NVP–*co*–$BVIM^+Cl^-$) hereafter, exhibits very good solubility in 1-butyl-3-methylimidazolium tetrafluoroborate ([BMIM][BF_4]) IL [15] by simultaneously presenting almost the same functions as that of PVP. The IL-like copolymer affords excellent steric and elec-

* Corresponding author. Fax: +86 10 62751708.
E-mail address: yuankou@pku.edu.cn (Y. Kou).

0021-9517/$ – see front matter
doi:10.1016/j.jcat.2007.05.009

trostatic stabilization effects on the rhodium nanoparticles in benzene hydrogenation, giving a TTO of 20,000. We believe that the IL-like copolymer can be widely applied in various applications to protect extensive nanoparticles composed of different metals. The platinum catalyst reported here is thought to be a good example. Indeed, no matter what a stabilization strategy is considered, the balance between the activity and the stability of the nanoparticles rather than their stability is necessarily the aim of catalysis. Consequently, in this regard, "protection" (i.e., protecting the particles against aggregation) is a better word than "stabilization" to characterize this balance, because high selectivity, large TOF, and long lifetime are always expected in a catalytic reaction.

2. Experimental

2.1. Synthesis of the IL-like copolymer poly(NVP–co–BVIM$^+$Cl$^-$)

The IL-like copolymer poly(NVP–*co*–BVIM$^+$Cl$^-$) was prepared as described previously [15]. A typical procedure was as follows. In a 25-ml round-bottomed Schlenk flask equipped with a condenser and a magnetic stirrer, 18.50 g (200 mmol) of butyl chloride was added to 5.00 g (53 mmol) of 1-vinylimidazole. Under nitrogen atmosphere, the mixture was then refluxed for 24 h in an oil bath at 70 °C under vigorous stirring. After cooling to room temperature, the upper phase (mainly excess butyl chloride) was poured out, and the solid residue was washed three times using 30 ml of ethyl acetate. The residue was then dried in vacuum for 2 h at 60 °C to give the pale-yellow solid as a product (1-butyl-3-vinylimidazole chloride, [BVIM]$^+$Cl$^-$) (yield: 75%).

A mixture of *N*-vinyl-2-pyrrolidone (NVP, 1.856 g, 16.7 mmol), [BVIM]$^+$Cl$^-$ (1.558 g, 8.35 mmol), azobisisobutyronitrile (AIBN, 17.0 mg), and 5 ml of methanol was first degassed by about five freeze/thaw cycles and then placed in a preheated oil bath set at 60 °C with stirring. After 16 h, the now-solidified reaction mixture was diluted with an appropriate amount of methanol to stop the reaction. The mixture was added dropwise to 200 ml of ethyl ether, resulting in a pale-yellow precipitate. Residue monomers were removed from the precipitate by dialysis for 24 h in 500 ml × 3 methanol. After dialysis, the methanol solution involving the precipitate was heated under vacuum, and the final product was dried in vacuum at room temperature. A total of 2.326 g of yellow solid was obtained (yield: 68%). The purity and the copolymer compositions were checked by ^{1}H NMR spectroscopy.

2.2. Synthesis of 1-butyl-3-methylimidazolium tetrafluoroborate ([BMIM][BF$_4$]) IL

Butyl chloride (AR grade) was dried with P_2O_5 for 4 h and then distilled for use. 1-Butyl-3-methylimidazolium chloride ([BMIM]Cl) was prepared by the reaction of 70 ml of 1-methylimidazole (99%) and 300 ml of butyl chloride in a 500-ml Schlenck flask under nitrogen atmosphere (99.999%) at 70 °C for 24 h. The resulting viscous liquid was cooled to −20 °C overnight, after which the upper liquid phase (mainly excess butyl chloride) was decanted. The resulting white solid was dissolved in 15 ml of acetonitrile at 50 °C and then mixed with 200 ml of ethyl acetate. This mixture was then recrystallized at −20 °C overnight. The foregoing recrystallization procedure was repeated twice. After the second recrystallization, the remaining acetonitrile and ethyl acetate were removed at 70 °C at reduced pressure. To prepare [BMIM][BF$_4$], tetrafluoroboric acid aqueous solution (⩾40%) was added (slowly to prevent a significant temperature rise) to a mixture of [BMIM]Cl, 100 ml of water, and 200 ml of dichloromethane ([BMIM]Cl:tetrafluoroboric acid = 1:1.1, molar ratio). After stirring for 4 h, the lower IL portion was separated and washed with water (30 ml × 5) until a pH ≈ 7 was reached. No Cl$^-$ was found by $AgNO_3$ detection. [BMIM][BF$_4$] was heated under vacuum at 60 °C for 2 h and then further dried under vacuum at 60 °C for 24 h to remove any excess solvent (total yield: 64%).

2.3. Preparation of platinum nanoparticles

Two kinds of platinum nanoparticles were prepared: hydrogen-reduced platinum nanoparticles and ethylene glycol-reduced platinum nanoparticles. In a typical experiment, the hydrogen-reduced platinum nanoparticles (designated **Pt-I**), 1.85 ml $H_2PtCl_6{\cdot}6H_2O$ (1.93×10^{-2} M, 3.6×10^{-5} mol) aqueous solution and 1.87 ml poly(NVP–*co*–BVIM$^+$Cl$^-$) (9.73×10^{-2} M, average monomer molecular weight 126.2, 1.8×10^{-4} mol as monomeric unit) methanol solution were added to 6 ml [BMIM][BF$_4$] (poly(NVP–*co*–BVIM$^+$Cl$^-$):Pt = 5:1). The mixture solution was heated under vacuum at 60 °C for 2 h to remove water and methanol, then reduced under 4.0 MPa H_2 at 80 °C for 30 min in an autoclave with a stirring speed of 800 rpm. The resulting black solution containing copolymer-stabilized platinum nanoparticles was used for the hydrogenation of *o*-CNB.

The ethylene glycol-reduced platinum nanoparticles (designated as **Pt-II**) were prepared as described previously [32]. First, 5 ml of ethylene glycol solution of NaOH (0.5 M, 2.5×10^{-3} mol) was added to 5 ml of ethylene glycol solution of $H_2PtCl_6{\cdot}6H_2O$ (1.93×10^{-4} mol). The mixture was then heated to 160 °C for 3 h, with an Ar flow passing through the reaction system to take away water and organic byproducts. A transparent dark-brown homogeneous solution of the platinum nanoparticles was obtained. In a typical hydrogenation experiment, a 0.19-ml ethylene glycol solution of platinum nanoparticles (3.6×10^{-6} mol Pt) and a 0.19-ml poly(NVP–*co*–BVIM$^+$Cl$^-$) methanol solution (0.0973 M, 1.8×10^{-5} mol) were added to 6 ml of [BMIM][BF$_4$]. The mixture solution was heated under vacuum at 60 °C for 30 min to remove methanol. The resulting solution was used for the hydrogenation of *o*-CNB.

2.4. Hydrogenation of o-CNB catalyzed by platinum nanoparticles in [BMIM][BF$_4$]

In typical experiments, 4.76 g of *o*-CNB (3.0×10^{-2} mol) was added to the copolymer-stabilized platinum nanoparticles

(either Pt-I or Pt-II). The hydrogenation reaction was carried out in a 60-ml autoclave under 4.0 MPa H_2 at 60 °C, at a stirring speed of 800 rpm. After the reaction (typically 1 h), 15 ml of ethyl ether was added to extract the products four times. The products were then analyzed by gas chromatography (GC), using an Agilent 6820 equipped with a 30-m HP-INNOWax capillary column and a flame ionization detector and GC–mass spectrometry (GC–MS), using a Finnigan-MAT GCQ. The residual [BMIM][BF_4] solution (containing platinum nanoparticles) was heated under vacuum at 60 °C for 30 min and then used for recycling.

2.5. Inductively coupled plasma-atomic emission spectroscopy measurements

The platinum leaching during ethyl ether extraction was analyzed by inductively coupled plasma-atomic emission spectroscopy (ICP-AES) as follows: The obtained ethyl ether solution was initially heated under vacuum to remove ethyl ether. Then 10 ml of HNO_3 and 30 ml of HCl were added. The mixture was fluxed at 100 °C overnight until the platinum metal was thoroughly dissolved. Then the resulting transparent solution was diluted to 500 ml by deionized water and used for the ICP-AES measurement (PROFILE SPEC, LEEMAN LABS; detection limit ∼1 μg-ng/ml).

2.6. Infrared spectrum characterizations

The appropriate amount of *o*-CNB (volume ratio about 1/3–1/10) was heated to liquid, and mixed with ethyl ether, methanol, [BMIM][BF_4], and the Pt-I solution. Then one drop of each sample was spread on the KBr windows and used for the infrared (IR) measurements. All experiments were performed on a Bruker Vector 22 Fourier transform infrared spectrometer with a resolution of 2 cm^{-1}.

2.7. Transmission electron microscopy characterizations

The transmission electron microscopy (TEM) measurements were carried out on a Hitachi H-9000 electron microscopy operated at 300 kV. The samples were prepared as follows. First, the appropriate mount of deionized water was added to the solutions containing platinum nanoparticles, followed by centrifugation. The resulting platinum nanoparticles were dried under vacuum at 70 °C for 24 h to remove any solvents, which were used for TEM and XRD measurements. The samples thus obtained were appropriately diluted with deionized water (∼1 mg/ml) and dispersed by ultrasonication for more than 2 h. Then one drop of solution was placed on a copper grid coated by a polymer or carbon film. The excess solution was removed by adsorbent paper. The average particle sizes of the platinum nanoparticles were determined from more than 200 nanoparticles.

2.8. X-ray diffraction analysis

The X-ray diffraction (XRD) samples were prepared as described in the previous section. All XRD patterns were recorded on a Rigaku D/MAX-2400 diffractometer using Cu $K\alpha$ radiation ($\lambda = 1.5406$ Å) operated at 30 kV and 100 mA. The average particle sizes (D) were estimated by Scherrer's equation [33], $D = 0.90\lambda/(\beta\cos\theta)$, where θ is the diffraction angle and β is the full width at half-maximum.

3. Results and discussion

3.1. Platinum catalyst recovery

Using [BMIM][BF_4] IL as the solvent could not stabilize the platinum nanoparticles due to the obvious precipitation. When an appropriate amount of the copolymer (poly(NVP–*co*–$BVIM^+Cl^-$):Pt = 5:1, molar ratio) was added, however, the uniform colloidal platinum nanoparticles could be obtained easily, implying that the addition of copolymer is essential to protect the particles. The copolymer-stabilized platinum nanoparticles, which could not be isolated by centrifugation at 12,000 rpm for 30 min, were very stable. No precipitate was observed even after standing for 6 months, and no aggregation was observed after the reaction. Thus, product separation and catalyst recycling could be easily done by simple ethyl ether extraction and decantation, as illustrated in Fig. 1. The catalyst leaching in this process was negligible. The platinum loss was under the detection limit (∼1 ng-μg/ml) of standard ICP-AES analysis. The recovered catalysts were heated under vacuum to remove excessive solvent and then reused for the next run.

3.2. Hydrogenation performance in a single cycle

Based on GC and GC-MS analysis, *o*-CAN was the main product, giving aniline (AN) as the main byproduct. The hydrogenation results from the first cycle are shown in Table 1. For the Pt-I (entries 1–2), as the *o*-CNB/Pt molar ratio increased from 833 to 8330, the turnover frequency (TOF) rose from 778 to 7697 h^{-1} with improved selectivity (96.2 to 98.0%), indicating that the reaction rate is greatly controlled by mass transport. Anthony et al. [34] and Dyson et al. have suggested that the low solubility of hydrogen gas in ILs may lead to mass-transfer problems in catalytic reactions [35]. The concentration of hydrogen in ILs appeared to control the reaction rate, resulting in increased TOF when the amount of platinum was decreased. When the Pt-II catalyst was applied (entry 3), a slightly lower TOF (6639 h^{-1}) with a preserved selectivity (99.1%) was observed. It is noteworthy that the reaction rates (or TOF) and the selectivities of both Pt-I and Pt-II catalysts were much higher than those of conventional PVP-Pt catalyst (217–701 h^{-1} and 45.3–46.0%, respectively; see entries 5 and 6).

The improved selectivity may be due to the use of ILs, which reportedly enhance selectivity and/or inhibit dehalogenation in catalytic hydrogenation compared with conventional organic solvents [30,31]. In fact, before the use of ILs, Yu and Liu [19] and Yang et al. [20] had already proposed that the addition of some metal cations might result in better selectivity in *o*-CNB hydrogenation catalyzed by PVP–Pt system. They suggested that the metal cations might have a weak interaction with

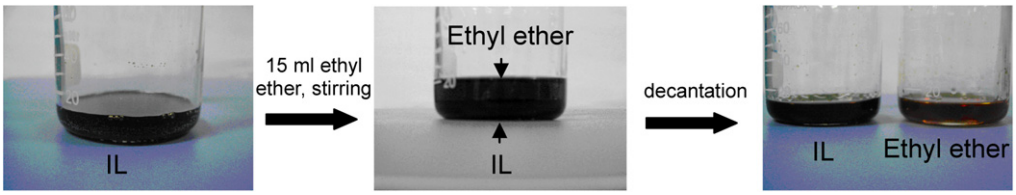

Fig. 1. The simple product separation and the catalyst recovery by ethyl ether extraction.

Table 1
Catalytic activities of the *o*-CNB hydrogenation catalyzed by Pt nanoparticles in a single cycle[a]

Entry	Catalyst	*o*-CNB:Pt	Time (h)	*o*-CNB conversion (%)	Selectivity (%)			TOF (h^{-1})
					o-CAN	AN	Others	
1	Pt-I	833	0.83	77.5	96.2	2.6	0.9	778
2[b]	Pt-I	8330	1.0	92.4	99.7	Trace	0.3	7697
3[b]	Pt-II	8330	1.0	79.7	99.1	0.5	0.4	6639
4	Blank	–	1.0	3.9	96.4	3.6	Trace	–
5[c]	PVP–Pt	126	0.58	100	45.3	43.4	11.3	217
6[d]	PVP–Pt	379	0.54	97.2	46.0	0.2	53.8	701

[a] Typical reaction conditions: 6 ml [BMIM][BF_4], 3.6×10^{-5} mol Pt, 30 mmol *o*-CNB, 60 °C, 4 MPa H_2, poly(NVP–*co*–BVIM$^+$Cl$^-$):Pt = 5:1.
[b] 3.6×10^{-6} mol Pt.
[c] From Ref. [36]. Reaction conditions: 25 ml methanol, 60 °C, 0.1 MPa H_2.
[d] From Ref. [17]. Reaction conditions: 4.49×10^{-6} mol PVP–Pt colloid, 1.70×10^{-3} mol *o*-CNB, 0.10 ml *n*-decanol (internal standard for GC) and 4.49×10^{-6} mol metal salt; 0.1 MPa H_2 and 30 °C (the whole volume was 15.0 ml, MeOH).

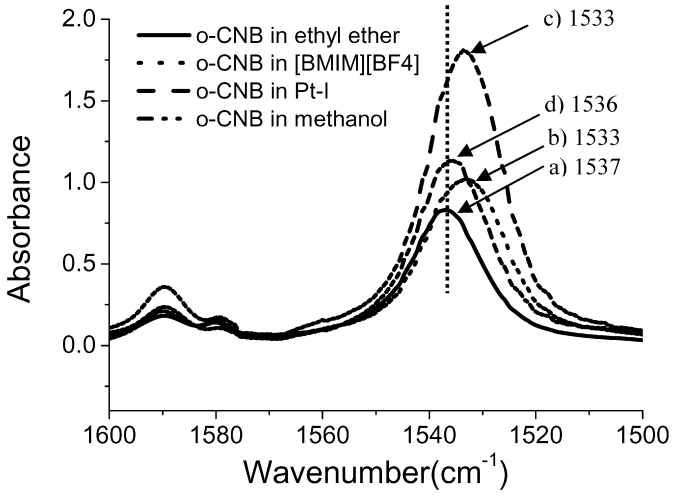

Fig. 2. The IR spectra of the asymmetric stretch vibrations of the nitro groups of *o*-CNB in: (a) ethyl ether; (b) [BMIM][BF_4]; (c) Pt-I; and (d) methanol.

the nitro group of *o*-CNB by adsorbing on the platinum catalyst surface. Consequently, it is of interest to know whether the [BMIM][BF_4] IL used here (i.e., the imidazolium cations) may interact with *o*-CNB in a way somewhat similar to that of those metal cations.

To shed light on this point, a series of IR characterizations were carried out, as shown in Fig. 2. The asymmetric stretch vibration of the nitro (O=N=O) group of *o*-CNB [37], which is at 1537 cm^{-1} (a) in ethyl ether solvent (1550 cm^{-1} for gas-phase *o*-CNB [38]), shifted to 1533 cm^{-1} (b) in [BMIM][BF_4], implying that the N=O bond of *o*-CNB was further weakened by the IL. To exclude any possible long-range or short-range intermolecular interactions caused by either the IL-like copolymer or the platinum nanoparticles, an appropriate amount of *o*-CNB was added to the freshly prepared Pt-I catalyst in [BMIM][BF_4]. The observation of the same shift to 1533 cm^{-1} (c) clearly indicates that [BMIM][BF_4] was responsible for the red-shift of the nitro group vibrational frequency. On the other hand, the *o*-CNB dissolved in methanol (d) showed almost no such shift (1537 to 1536 cm^{-1}), indicating that there are much stronger molecular interactions of the nitro group of *o*-CNB with the [BMIM][BF_4] IL.

To better understand the interactions between [BMIM][BF_4] and *o*-CNB at the molecular level, density functional theory (DFT) calculations were performed using the Gaussian 03 program package [39]. All geometry optimizations and frequency calculations were carried out with the B3LYP density functional level of theory (Becke's three-parameter nonlocal exchange functional [40] with the correlation functional of Lee et al. [41,42]), in conjugation with the 6-31G(d) basis set. The single point energies and Gibbs free energies were further calculated at the B3LYP/6-311++G(2d,p) level. Although the B3LYP method lacks the terms describing dispersion force, its reproduction of the structures of hydrogen-bonded liquids and ILs is surprisingly very good, at least better than that of most empirical models [43,44]. Ideally, the continuum solvation models, such as the polarizable continuum model (PCM), would be a good choice for calculation of the solvation effects. But because many necessary physiochemical parameters (e.g., the temperature dependence of a dielectric constant, molecular radius, molar volume) are not immediately available at the present stage (except for the Onsager model, which is rather coarse and unreliable, however), calculation of the solvation effects in ILs using continuum solvation models has not yet been reported. Therefore, we had to use several gas-phase con-

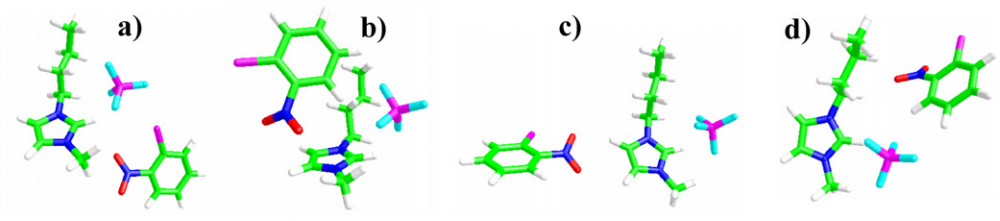

Fig. 3. Four configurations (a, b, c, and d) of the intermolecular interactions between *o*-CNB and [BMIM][BF_4] optimized at the B3LYP/6-31G(d) level.

Table 2
The energies and IR frequencies obtained by DFT calculations

Configuration	Relative energy (kcal/mol)[a]		Frequency (cm^{-1})[b]	
	B3LYP/6-31G(d)	B3LYP/6-311++G(2dp)//B3LYP/6-31G(d)	O=N=O asymmetric stretch	C–Cl stretch
o-CNB[c]	–	–	1598	708
a	0	0	1589	710
b	−5.3	−3.6	1582	707
c	−1.5	−2.3	1590	710
d	−4.9	−4.4	1587	706

[a] Gibbs free energy at 298 K, not scaled.
[b] Calculated at the B3LYP/6-31G(d) level. The standard scale factor of 0.9614 was used [45].
[c] Isolated gas-phase *o*-CNB calculated at the B3LYP/6-31G(d) level.

figurations consisting of one [BMIM][BF_4] molecule and one *o*-CNB molecule to simulate the solvation effects. The fact that the anions of ILs were usually found at the side of 2-H of the imidazolium ring [43] encouraged us to use this structure directly when constructing the initial configurations. Overall, five possible positions of *o*-CNB relative to the imidazolium ring were considered: above (one configuration, a), below (one configuration, b), and at the side (three configurations, c–e) of the ring, as illustrated in Fig. 1S in Supporting material. After fully geometrical optimizations, four configurations indicating the most possible interactions of *o*-CNB with the imidazolium ring, three at the side (a, c, d) and one above the ring (b) (see Fig. 3) were finally obtained. As shown in Table 2, the difference between the Gibbs free energies (298 K) of four configurations is only 0–4.4 kcal/mol at the B3LYP/6-311++G(2dp)//B3LYP/6-31G(d) level [0–5.3 kcal/mol at the B3LYP/6-31G(d) level], which approaches the error range of solvation effects. The configuration e was not stable and finally became to be identical with the configuration a. In four configurations, the nitro groups are obviously closer to the imidazolium rings compared with the chloride atoms, indicating the strong interaction of the nitro groups in the *o*-CNB with the rings of imidazolium. The fact that the four configurations are not distinguishable from one another suggests that the intermolecular interactions between [BMIM][BF_4] and *o*-CNB are somewhat more complicated than what we estimated earlier.

The asymmetric stretch vibrational frequencies of nitro groups were also tabulated. A standard scaling factor (0.9614) suggested by Scott and Radom [45] was used to obtain the fundamental vibrations (i.e., the stretch vibrations of nitro groups and C–Cl bonds). For the isolated gas-phase *o*-CNB, the asymmetric stretch vibrational frequency of nitro group was calculated to be 1598 cm^{-1}, very close to the experimental value of 1550 cm^{-1}, implying that the B3LYP/6-31G(d) method is reliable for this system. Compared with that of gas phase *o*-CNB, the frequency calculation of the four configurations (a–d in Fig. 3) gave red-shifts of 8–16 cm^{-1} for the nitro groups in [BMIM][BF_4], in good agreement with the above experimental value (red-shift ∼17 cm^{-1}). The red-shifts of the four configurations demonstrate that the N=O bonds of nitro groups were weakened by the imidazolium cations of ILs. On the other hand, the C–Cl bond stretch vibrational frequencies showed almost no shifts ($-2 \sim +2$ cm^{-1}), implying that the C–Cl bonds were preserved. In accordance with the above results obtained at the B3LYP/6-31G(d) level, it is noteworthy that the calculations at the B3LYP/3-21G(d) level (see Fig. 2S and Table 1S in Supporting material) gave red-shifts of 7–14 cm^{-1} for the nitro groups but almost no shifts ($-2 \sim +6$ cm^{-1}) for the C–Cl bonds, indicating that the calculated relative frequencies are insensitive to the basis sets and thus are useful in gaining a better understanding of the weakening of N=O bonds toward the significant improvement in *o*-CAN selectivity.

3.3. Catalyst recycling

To test the recyclability of the platinum nanoparticles, the Pt-I catalyst was recycled 17 times, as shown in Table 3. The high selectivities (95.1–99.9%) were preserved throughout recycling. It is noteworthy that the TOF remained unchanged until the seventh run. After 17 runs, the TOF decreased by only about 15% with respect to that of the fresh catalyst (659 vs 778 h^{-1}), giving a TTO of 12,296. However, on increasing the *o*-CNB/Pt molar ratio from 833 to 8330 for Pt-I, the catalyst quickly deactivated. As shown in Table 4, the TOF decreased immediately from 7697 to 4248 h^{-1} at the second run and then further to 1995 h^{-1} at the third run (entries 1–3). Even after the amount of the IL-like copolymer was increased with the hope of slowing the catalyst deactivation rate, the TOF was maintained (with difficultly) only until the third run (entries 4–6). Meanwhile, the TTO was not improved by the addition of more copolymer (13,940 and 11,654, respectively).

The above results suggest that more stable nanoparticles (i.e., longer lifetime) may certainly lead to lower TOF (i.e., lower substrate/catalyst ratio, higher stabilizer concentration). That is, simple enhancement of particle stability may be an ineffective approach to obtaining high TTO, because controlling the balance between catalytic activity and stability is necessarily the aim of catalysis. In this regard, we prepared another platinum nanoparticle catalyst, Pt-II, by ethylene glycol reduc-

Table 3
The recycle results of the *o*-CNB hydrogenation catalyzed by Pt-I (*o*-CNB:Pt = 833)[a]

Run	Time (h)	*o*-CNB conversion (%)	Selectivity (%)			TOF (h^{-1})
			o-CAN	AN	Others	
1	0.83	77.5[b]	96.5	2.6	0.9	778
2	1.0	94.6	95.1	1.4	3.5	788
3	1.0	94.8	99.1	0.4	0.5	790
4	1.0	95.9	99.1	0.4	0.5	799
5	1.0	95.6	98.2	0.2	1.6	796
6	1.0	93.4	99.4	0.1	0.5	778
7	1.0	81.9	99.6	0.2	0.2	682
8	1.0	86.4	99.8	Trace	0.2	720
9	1.0	86.4	99.9	0.1	Trace	720
10	1.0	85.0	99.8	Trace	0.2	708
11	1.0	81.9	98.3	Trace	1.7	682
12	1.0	81.8	99.9	Trace	0.1	681
13	1.0	86.6	98.4	Trace	1.6	721
14	1.0	83.9	99.9	Trace	0.1	699
15	1.0	76.6	99.9	Trace	0.1	638
16	1.0	78.9	99.9	Trace	0.1	657
17	1.0	79.1	99.0	Trace	1.0	659

[a] Reaction conditions: 6 ml [BMIM][BF_4], 3.6×10^{-5} mol Pt, 30 mmol *o*-CNB, 60 °C, 4 MPa H_2, poly(NVP–*co*–VBIM$^+$Cl$^-$):Pt = 5:1.
[b] Due to the shorter reaction time.

Table 4
The recycle results of the *o*-CNB hydrogenation catalyzed by Pt-I (*o*-CNB:Pt = 8330)[a]

Entry	Run	Time (h)	*o*-CNB conversion (%)	Selectivity (%)			TOF (h^{-1})
				o-CAN	AN	Others	
1[b]	1	1.0	92.4	99.7	Trace	0.3	7697
2[b]	2	1.0	51.0	99.8	Trace	0.2	4248
3[b]	3	2.0	47.9	99.3	Trace	0.7	1995
4[c]	1	1.0	55.8	99.9	Trace	0.1	4648
5[c]	2	1.0	58.7	99.9	Trace	0.1	4890
6[c]	3	1.0	25.4	99.9	Trace	0.1	2116

[a] Reaction conditions: 6 ml [BMIM][BF_4], 3.6×10^{-6} mol Pt, 30 mmol *o*-CNB, 60 °C, 4 MPa H_2.
[b] Poly(NVP–*co*–VBIM$^+$Cl$^-$):Pt = 5:1.
[c] Poly(NVP–*co*–VBIM$^+$Cl$^-$):Pt = 50:1.

Table 5
The recycling results of the *o*-CNB hydrogenation catalyzed by Pt-II (*o*-CNB:Pt = 8330)[a]

Run	Time (h)	*o*-CNB conversion (%)	Selectivity(%)			TOF (h^{-1})
			o-CAN	AN	Others	
1	1.0	79.7	99.1	0.5	0.4	6639
2	1.0	84.2	98.4	0.1	1.5	7014
3	1.0	76.5	97.5	0.2	2.3	6372
4	1.0	70.8	97.5	Trace	2.5	5898

[a] Reaction conditions: 6 ml [BMIM][BF_4], 3.6×10^{-5} mol Pt, 30 mmol *o*-CNB, 60 °C, 4 MPa H_2, poly(NVP–*co*–VBIM$^+$Cl$^-$):Pt = 5:1.

tion. Table 5 shows that the Pt-II catalyst displayed much higher reactivity (7014–5898 h^{-1}) with very high selectivity (97.5–99.1%). Thus, the unprecedented TTO (>25,900) was obtained after only 4 runs.

To identify the reason for the much better performance of the Pt-II catalyst, TEM and XRD characterizations were carried out on both catalysts. Fig. 4 demonstrates that the freshly prepared and recovered Pt-I catalysts had average particle sizes of 5.1 ± 1.1 nm and 5.6 ± 1.2 nm, respectively; and the fresh and recovered Pt-II catalysts had average particle sizes of only 1.7 ± 0.4 nm and 2.3 ± 0.4 nm, together with much narrower distributions. Both the catalysts showed a size increase of 0.5–0.6 nm after recycling. Meanwhile, XRD analysis was performed by precipitating and centrifuging the platinum nanoparticles after an appropriate amount of water was added (see Section 2 for details). The diffraction patterns are shown in Fig. 5. The diffraction lines of (111) (0.2258 nm), (200) (0.1962 nm), (220) (0.1388 nm), and (311) (0.1182 nm) of metallic platinum repeatedly and clearly seen for the Pt-I and Pt-II catalysts demonstrate that the catalysts have the same fcc crystal structure [46]. The average particle sizes before and after running estimated by the (111) diffraction lines, given in Table 6 (with the TEM results also tabulated for comparison), indicate increase from 6.7 to 7.3 nm for Pt-I and from 3.3 to 3.8 nm for Pt-II. Because the particles smaller than 3 nm are in principle XRD-invisible, these XRD results are considered in full agreement with the TEM observations. The increase in average particle size is possibly due to the Ostwald ripening process, which is also in agreement with the observations on palladium nanoparticles in the Suzuki reaction reported by Narayanan and El-Sayed [47]. In all, the foregoing characterizations demonstrate that (1) protection of smaller Pt nanoparticles (which should have better activity in catalysis) by the IL-like copolymer is not more difficult (in fact, the Pt-II catalyst with smaller average particle size appears to live much longer than the Pt-I catalyst), and (2) aggregation of the nanoparticles after recycling, which surely leads to an decrease in catalytic activity, will remain an open question for a very long run time as well as a very large TTO (e.g., >30,000–50,000).

4. Conclusion

[BMIM][BF_4] and the IL-like copolymer poly(NVP–*co*–BVIM$^+$Cl$^-$) can provide excellent co-stabilization effects for the platinum nanoparticles. In accordance with our previous work on rhodium nanoparticles, we believe that this stabilization strategy can be extensively applied in the preparation of various catalytically highly active nanoparticles covering all transition metals.

Using [BMIM][BF_4] as the solvent and poly(NVP–*co*–BVIM$^+$Cl$^-$) as the stabilizer is a good solution for the *o*-CNB hydrogenation catalyzed by the platinum nanoparticles. [BMIM][BF_4] is advantageous not only for product separation and catalyst recycling, but also for selectivity improvement. The IR spectra and DFT calculations reveal that the intermolecular interactions between the imidazolium cation of [BMIM][BF_4] and the nitro group of *o*-CNB induced a weakened N=O bond, resulting in an obvious red-shift on the asymmetric stretch vibration of the O=N=O group. DFT calculations also show that the intermolecular interactions of [BMIM][BF_4] and *o*-CNB did not weaken the C–Cl bonds.

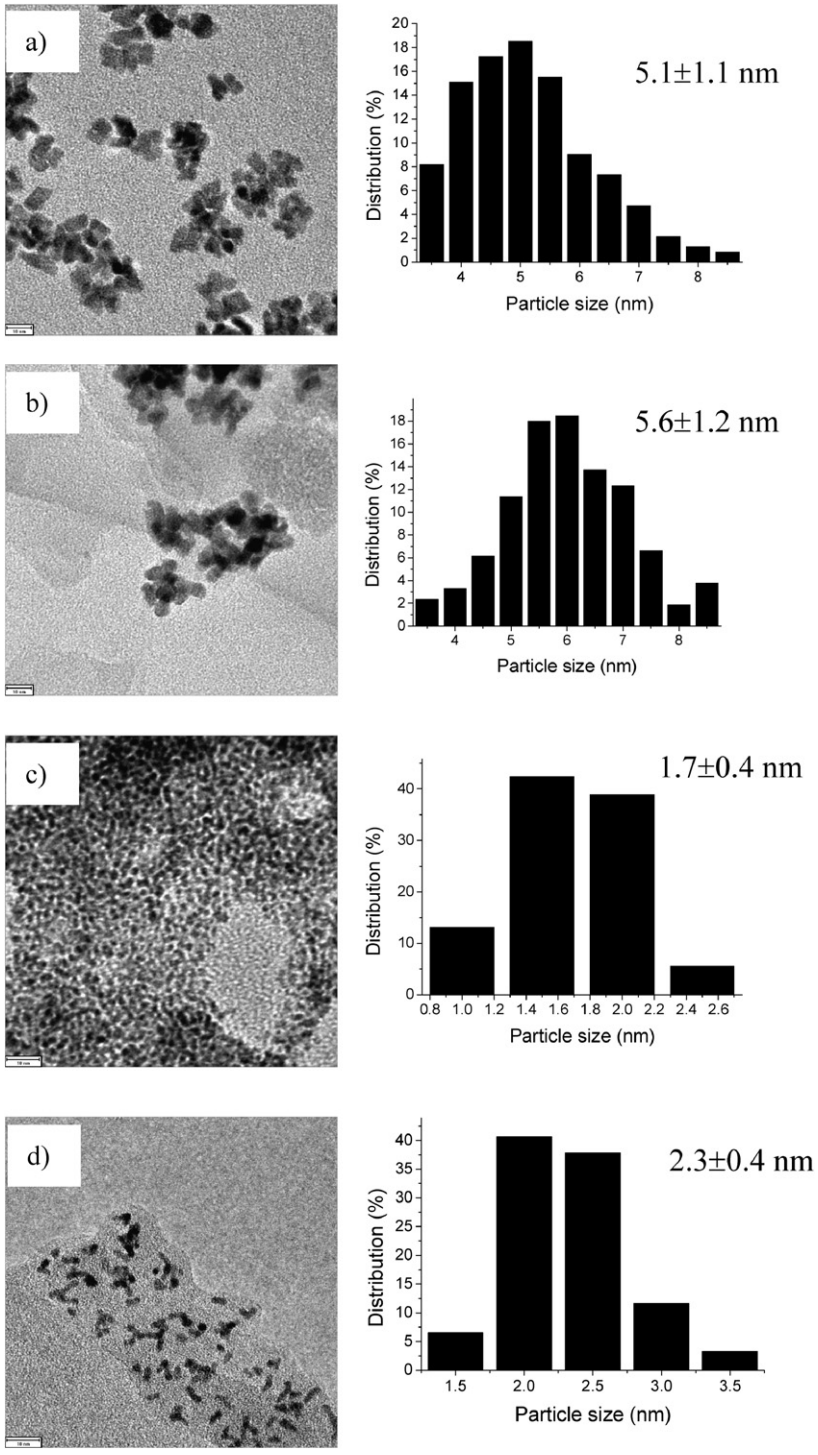

Fig. 4. TEM micrographs (scale bar = 10 nm) and size distributions of (a) fresh Pt-I; (b) recovered Pt-I after the reaction (*o*-CNB/Pt = 833); (c) fresh Pt-II; and (d) recovered Pt-II after the reaction (*o*-CNB/Pt = 833).

The different effects on N=O bonds and C–Cl bonds caused by [BMIM][BF_4] may be responsible for the enhanced *o*-CAN selectivity.

TEM and XRD characterizations demonstrate that the average particles sizes of both Pt-I and Pt-II increased by about 0.5–0.6 nm after the reaction, possibly due to the Ostwald ripening process. The increase in average particle size will eventually lead to the aggregation of nanoparticles, resulting in the catalyst deactivation. In this regard, smaller nanoparticles will live longer, a conclusion supported by the excellent performance of the Pt-II with an unprecedented TTO (>25,900).

Acknowledgments

This work was supported by the National Science Foundation of China (Projects 20533010 and 20473002). The authors

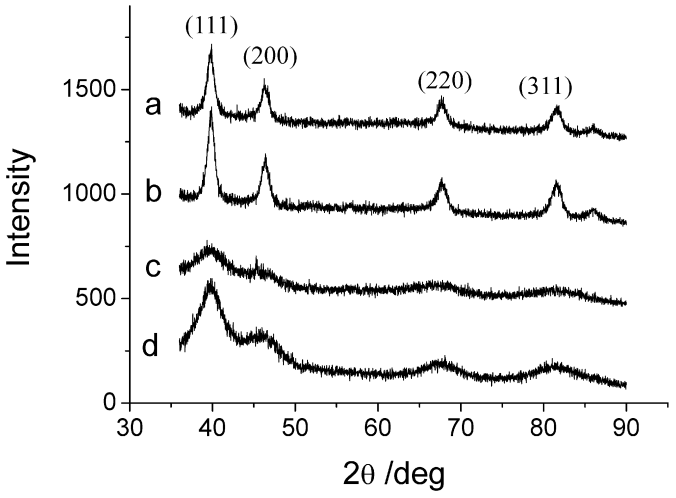

Fig. 5. XRD diffraction patterns of (a) fresh Pt-I; (b) recovered Pt-I after the reaction (*o*-CNB/Pt = 833); (c) fresh Pt-II; (d) recovered Pt-II after the reaction (*o*-CNB/Pt = 833).

Table 6
The average particle sizes of platinum nanoparticles measured by TEM and XRD (unit: nm)

Method	Pt-I		Pt-II	
	Fresh	Recovered	Fresh	Recovered
TEM	5.1 ± 1.1	5.6 ± 1.2	1.7 ± 0.4	2.3 ± 0.4
XRD	6.7	7.3	3.3	3.8

thank Professors Wenjian Liu and Yundong Wu, Peking University, for the helpful discussions on theoretical approaches.

Supporting material

The online version of this article contains additional supplementary material.

Please visit DOI:10.1016/j.jcat.2007.05.009.

References

[1] G. Schmid, Chem. Rev. 92 (1992) 1709.
[2] R.G. Finke, in: D.L. Feldheim, C.A. Foss Jr. (Eds.), Transition-Metal Nanoclusters, Dekker, New York, 2002, chap. 2, p. 17.
[3] A. Roucoux, J. Schulz, H. Patin, Chem. Rev. 102 (2002) 3757.
[4] J.D. Aiken III, R.G. Finke, J. Mol. Catal. A Chem. 145 (1999) 1.
[5] H. Bönnemann, R.M. Richards, Eur. J. Inorg. Chem. (2001) 2455.
[6] D. Astruc, F. Lu, J.R. Aranzaes, Angew. Chem. Int. Ed. 44 (2005) 7852.
[7] Y. Wang, N. Toshima, J. Phys. Chem. B 101 (1997) 5301.
[8] Y. Lin, R.G. Finke, J. Am. Chem. Soc. 116 (1994) 8335.
[9] J.D. Aiken, R.G. Finke, J. Am. Chem. Soc. 121 (1999) 8803.
[10] J.A. Widegren, R.G. Finke, J. Mol. Catal. A Chem. 191 (2003) 187.
[11] J.A. Widegren, R.G. Finke, J. Mol. Catal. A Chem. 198 (2003) 317.
[12] J.D. Aiken III, Y. Lin, R.G. Finke, J. Mol. Catal. A Chem. 114 (1996) 29.
[13] C.W. Scheeren, G. Machado, J. Dupont, P.F.P. Fichtner, S.R. Texeira, Inorg. Chem. 42 (2003) 4738.
[14] J. Dupont, G.S. Fonseca, A.P. Umpierre, P.F.P. Fichtner, S.R. Teixeira, J. Am. Chem. Soc. 124 (2002) 4228.
[15] X.D. Mu, J.Q. Meng, Z.C. Li, Y. Kou, J. Am. Chem. Soc. 127 (2005) 9694.
[16] N. Yan, C. Zhao, C. Luo, P.J. Dyson, H. Liu, Y. Kou, J. Am. Chem. Soc. 128 (2006) 8714.
[17] X. Yang, H. Liu, Appl. Catal. A 164 (1997) 197.
[18] M. Liu, W. Yu, H. Liu, J. Mol. Catal. A Chem. 138 (1999) 295.
[19] W. Yu, H. Liu, J. Mol. Catal. A Chem. 243 (2006) 120.
[20] X. Yang, Z. Deng, H. Liu, J. Mol. Catal. A Chem. 144 (1999) 123.
[21] X.X. Han, R.X. Zhou, G.H. Lai, B.H. Yue, X.M. Zheng, React. Kinet. Catal. Lett. 81 (2004) 41.
[22] J.S. Wilkes, in: P. Wasserscheid, T. Welton (Eds.), Ionic Liquids in Synthesis, Wiley–VCH, Weinheim, 2003, chap. 1, p. 1.
[23] T. Welton, Chem. Rev. 99 (1999) 2071.
[24] J. Dupont, R.F. de Souza, P.A.Z. Suarez, Chem. Rev. 102 (2002) 3667.
[25] G.H. Tao, L. He, W.S. Liu, L. Xu, W. Xiong, T. Wang, Y. Kou, Green Chem. 8 (2006) 639.
[26] D.B. Zhao, M. Wu, Y. Kou, E. Min, Catal. Today 74 (2002) 157.
[27] C.C. Tzschucke, C. Markert, W. Bannwarth, S. Roller, A. Hebel, R. Haag, Angew. Chem. Int. Ed. 41 (2002) 3964.
[28] P. Wasserscheid, W. Keim, Angew. Chem. Int. Ed. 39 (2000) 3772.
[29] E.T. Silveira, A.P. Umpierre, L.M. Rossi, G. Machado, J. Morais, G.V. Soares, I.J.R. Baumvol, S.R. Teixeira, P.F.P. Fichtner, J. Dupont, Chem. Eur. J. 10 (2004) 3734.
[30] D.B. Zhao, P.J. Dyson, G. Laurenczy, J.S. McIndoe, J. Mol. Catal. A Chem. 214 (2004) 19.
[31] D.Q. Xu, Z.Y. Hu, W.W. Li, S.P. Luo, Z.Y. Xu, J. Mol. Catal. A Chem. 235 (2005) 137.
[32] Y. Wang, J. Ren, K. Deng, L. Gui, Y. Tang, Chem. Mater. 12 (2000) 1622.
[33] A. Guinier, Theorie et Technique de la Radiocristallographie, third ed., Dunod, Paris, 1964, p. 482.
[34] J.L. Anthony, E.J. Maginn, J.F. Brennecke, J. Phys. Chem. B 106 (2002) 7315.
[35] P.J. Dyson, G. Laurenczy, A. Ohlin, J. Vallance, T. Welton, Chem. Commun. (2003) 2418.
[36] J. Zhang, Y. Wang, H. Ji, Y. Wei, N. Wu, B. Zuo, Q. Wang, J. Catal. 229 (2005) 114.
[37] R.J. Francel, J. Am. Chem. Soc. 74 (1952) 1265.
[38] NIST/EPA Gas-Phase Infrared Database, Standard Reference Data Program, Gaithersburg, MD, 2004.
[39] M.J. Frisch, G.W. Trucks, H.B. Schlegel, G.E. Scuseria, M.A. Robb, J.R. Cheeseman, J.A. Montgomery Jr., T. Vreven, K.N. Kudin, J.C. Burant, J.M. Millam, S.S. Iyengar, J. Tomasi, V. Barone, B. Mennucci, M. Cossi, G. Scalmani, N. Rega, G.A. Petersson, H. Nakatsuji, M. Hada, M. Ehara, K. Toyota, R. Fukuda, J. Hasegawa, M. Ishida, T. Nakajima, Y. Honda, O. Kitao, H. Nakai, M. Klene, X. Li, J.E. Knox, H.P. Hratchian, J.B. Cross, C. Adamo, J. Jaramillo, R. Gomperts, R.E. Stratmann, O. Yazyev, A.J. Austin, R. Cammi, C. Pomelli, J.W. Ochterski, P.Y. Ayala, K. Morokuma, G.A. Voth, P. Salvador, J.J. Dannenberg, V.G. Zakrzewski, S. Dapprich, A.D. Daniels, M.C. Strain, O. Farkas, D.K. Malick, A.D. Rabuck, K. Raghavachari, J.B. Foresman, J.V. Ortiz, Q. Cui, A.G. Baboul, S. Clifford, J. Cioslowski, B.B. Stefanov, G. Liu, A. Liashenko, P. Piskorz, I. Komaromi, R.L. Martin, D.J. Fox, T. Keith, M.A. Al-Laham, C.Y. Peng, A. Nanayakkara, M. Challacombe, P.M.W. Gill, B. Johnson, W. Chen, M.W. Wong, C. Gonzalez, J.A. Pople, Gaussian 03, Revision B.03, Gaussian, Inc., Pittsburgh, PA, 2003.
[40] A.D. Becke, J. Chem. Phys. 98 (1993) 5648.
[41] C. Lee, W. Yang, R.G. Parr, Phys. Rev. B 37 (1988) 785.
[42] B. Miehlich, A. Savin, H. Stoll, H. Preuss, Chem. Phys. Lett. 157 (1989) 200.
[43] Z. Meng, A. Dölle, W.R. Carper, J. Mol. Struct. 585 (2002) 119.
[44] E.J. Meijer, M. Sprik, J. Chem. Phys. 105 (1996) 8684.
[45] A.P. Scott, L. Radom, J. Phys. Chem. 100 (1996) 16502.
[46] W.F. McClune, Powder Diffraction File Alphabetical Index Inorganic Phase, JCPDS, Swarthmore, PA, 1980.
[47] R. Narayanan, M.A. El-Sayed, J. Phys. Chem. B 109 (2005) 12663.